Molecular Dynamics Simulations of the Polymerization of Aqueous Silicic Acid and Analysis of the Effects of Concentration on Silica Polymorph Distributions, Growth Mechanisms, and Reaction Kinetics

Niny Z. Rao and Lev D. Gelb*

Center for Materials Innovation and Department of Chemistry, Washington University in St. Louis, St. Louis, Missouri 63130

Received: February 24, 2004; In Final Form: June 7, 2004

We have performed large-scale molecular dynamics simulations of the polymerization of silicic acid in aqueous solution using the potential developed by Fueston and Garofalini [*J. Phys. Chem.* **1990**, *94*, 5351]. Seventeen simulations, with different water-to-silicon ratios and silicic acid concentrations, were each run for between 1.6 and 12.5 ns, at temperatures of 1500, 2000, and 2500 K. Water clearly acts as a catalyst in these simulations. When the water-to-silicon ratio is large, we find that the initial stages of the polymerization process are dominated by the conversion of monomers to dimers and addition of monomers to small clusters, while at longer times cluster−cluster aggregation is observed. Using data from simulations at different temperatures, the activation energies of condensation between silicic acid monomers were calculated at different water-to-silicon ratios and found to compare favorably with experimental results; an extrapolation (at constant density) of simulated reaction rates to ambient conditions (a temperature difference of more than 1200 K) agrees with experimental rates to within one order of magnitude.

I. Introduction

Sol−gel processing has been extensively studied experimentally[1−14] and with theoretical methods.[15−49] These studies have provided valuable knowledge about the structures of sol−gel materials. In this work, we will focus on the oligomerization of aqueous silicic acid, which proceeds via a water-producing condensation reaction:

$$(OH)_3Si{-}OH + HO{-}Si(OH)_3 \rightleftarrows (OH)_3Si{-}O{-}Si(OH)_3 + H_2O \quad (1)$$

The interactions between silicic acid and water have been studied using quantum-mechanical calculations at various level of theory.[12,19,21,32−34,38−41,45,50] It is widely believed that the condensation mechanism involves over-coordinated silicon intermediates for both acid-catalyzed and base-catalyzed reactions.[1] The energies of various configurations of silicic acid−water clusters have been computed in more recent studies to provide more insight into the reaction pathway.[18,26,29,31,37,39] These calculations support a condensation mechanism involving pentacoordinated silicon intermediates. Recent ab initio studies by Pereira et al. have considered two possible condensation reaction mechanisms.[39] The first is an S_N2-type nucleophilic attack in which the nucleophile (the oxygen in $Si(OH)_4$) attacks from the side opposite the leaving group (water), and the other is a lateral attack in which the leaving group is adjacent to the nucleophile. This study concluded that the S_N2 path is favored over the lateral attack mechanism because the pentacoordinated silicon intermediate formed in the lateral attack mechanism is less stable than that formed in the S_N2-type mechanism. Quantum-mechanical calculations such as these can only treat systems containing a few silicic acid and water molecules and thus are suitable for the investigation of reaction mechanisms, but cannot be used to probe the larger structures formed during gelation. The evolution of larger structures can be directly modeled using empirical potentials and molecular dynamics (MD) simulations.

Previous MD studies of silica gelation can be divided into two categories, which differ in the type of potential energy function (force field) used and whether chemical reactions are included explicitly (dynamically) or implicitly. Pereira et al. have used a nonreactive potential to simulate small silica clusters and solutions of water, methanol, ethanol, TMOS, and TEOS.[39−43] They have shown that the potentials implemented in the DISCOVER and DL_POLY simulation packages provide reasonably accurate descriptions of bulk water, methanol, ethanol, TMOS, and TEOS under the conditions normally used for sol−gel processing.[42] The density of each simulated system was found to be in good agreement with experiment at various temperatures and pressures. Experimental enthalpies of vaporization and radial distribution functions are also reproduced well by these potentials. To describe polymerization reactions with these nonreactive potentials, an indirect approach was taken. Three "stages" were considered: before hydrolysis, after hydrolysis but before condensation, and after condensation.[43] Close analyses of the radial distribution functions and the tendencies of species in each stage to aggregate lead Pereira et al. to conclude that condensation reactions between dimers (and presumably larger silica polymorphs) to form more complex silica clusters are favored over all other possible reactions.

The first molecular dynamics simulation of a sol−gel system using a reactive potential function was published by Garofalini et al. in 1986.[29] A solution consisting of water, silicic acid monomers, and dimers was simulated. The potential model consisted of a modified Born−Mayer−Huggins (BMH) potential

* Corresponding author. E-mail: gelb@wustl.edu.

10.1021/jp049169f CCC: $27.50
Published on Web 07/28/2004

to describe all Si−Si, Si−O, and O−O interactions in non-water molecules.[48] The O−O, O−H, and H−H interactions in water molecules were described using a modified Rahman−Stillinger−Lemberg (RSL2)-type potential.[51] Experimental studies have suggested that under neutral to acidic conditions (pH between 7 and 2), deprotonation of silicic acid monomers

$$H_4SiO_4 \rightleftarrows H_3SiO_4^- + H^+ \quad (2)$$

is the step leading to the water-producing condensation reaction.[1,11,27,30,39] This potential displayed such deprotonations and produced a reasonable description of silicic acid monomers and pyrosilicic acid dimers in aqueous solution. The energy of deprotonation of $Si(OH)_4$ into $H_3SiO_4^-$ was found to be in good agreement with previously published quantum-mechanical calculations.[38] However, this potential failed to produce condensation reactions. Instead, monomer pairs simply associated to form a complex with two pentacoordinated silicon atoms.

In 1990, Feuston and Garofalini modified the model to directly simulate sol−gel condensation.[27] The modified BMH potential was applied to all interactions present in the solution. The interactions between hydrogen and other types of atoms are supplemented by terms from the RSL2 potential.[51] A three-body term is also included which raises the energy whenever the angle between bonded atoms differs from the optimal angle. In the case of Si−O−Si, O−Si−O, and Si−O−H, the optimal angle is set to the tetrahedral angle. In the case of H−O−H, the angle is set to its experimental value of 104.5°. The ground-state structures of the water monomer, dimer, trimer, and a water-silicic acid cluster (one water molecule and one silicic acid monomer or dimer) obtained using this potential function are in good agreement with previous ab initio calculations.[27] Polymerization in a system containing 27 silicic acid monomers was simulated at high temperatures so that the expected reactions would occur on time-scales accessible by molecular dynamics, e.g., nanoseconds. The reaction of two monomers was first observed at 1500 K. The water-producing condensation of two silicic acids was initiated by the deprotonation of one, followed by the formation of a pentacoordinate silicon intermediate. This energetically unfavorable intermediate subsequently lost either an oxygen atom or a hydroxyl group in an S_N2-type reaction. After 20 ps at 2500 K, over 50% of the original silicic acid monomers had formed oligomers, the largest of which contained six silicon atoms. Ten water molecules were also found at the end of the simulation, consistent with polymerization via reactions 1, above.

A subsequent study by Garofalini and Martin repeated this calculation on a larger scale, using a system of 216 silicic acid monomers at densities of 1.4−1.6 g/cm^3.[31] They observed that linear clusters are formed before cyclic clusters and reported the time evolution of the concentrations of Q_n species in the system. A Q_n silicon is defined as a silicon atom bound to n bridging oxygen atoms.[6] The activation energy for the formation of Q_3 species determined in this study compared well with an experimental value[27] for the activation energy of gelation, defined as the state when the largest oligomer spans the system.

Garofalini and Martin[37] showed using the same model that a nonbridging oxygen atom with two or more hydrogens (e.g., $-OH_2$) is a better leaving group than a hydroxyl group. Again, the formation of linear clusters before cyclic clusters was observed. A possible explanation was proposed involving the number of bridging oxygen atoms around the over-coordinated silicon atoms in the intermediate. When there are multiple bridging oxygens in the intermediate, there is a tendency to break a silanol bond rather than to lose a nonbridging oxygen atom. These observations are consistent with experimental studies of acid-catalyzed sol−gel solutions,[1,11] the conditions of which favor the formation of linear clusters.

The systems described in these studies were quite small ($N \leq 216$) and of relatively high density (1.3 g/cm^3 and above). The temperature and pressure conditions used are comparable with those of an autoclave process used to produce aerogels.[1,31,37] The initial configuration contained no water. These are not typical laboratory conditions for the preparation of sol−gel-derived materials. Usually, the alkoxide concentration used is relatively low, between 5 and ∼50 vol %.[1] The water-to-silicon ratio, r, is always greater than 1.0, and most work is done at near-ambient temperature and pressure.

We note that an entirely different approach to simulations of gelation can be taken using "Dynamic Monte Carlo" (DMC), which is essentially a stochastic integration of the chemical kinetics of the gelling system.[52] This method has been used with notable success in understanding the onset of gel formation, first-shell substitution effects, and the influence of cyclization in silicon alkoxide systems.[53−55] However, these methods require as input the various reaction rates and have not, to date, been applied in such a way as to include the instantaneous positions and diffusion of each polymorph, which would be necessary to generate an actual, physical model of a silica gel.

In the work presented here, molecular dynamics simulations of the polymerization of silicic acid in aqueous solution are carried out for systems containing 729 silicic acid monomers using the Feuston and Garofalini (FG) model. Our principle focus is on the structures formed during time-scales accessible to direct molecular simulation, rather than the chemistry of individual oligomerization events. Although these are small systems, they are large enough to provide information about the growth and structure of sol particles of size up to a few nanometers. NMR data indicate that the presence of excess water greatly affects the size and shape of particles in silica sols.[1] Many systems are considered here, varying both the water/alkoxide ratio, r, and the alkoxide density. In addition, simulations are carried out for a much longer time than in previous studies and at several temperatures. The time evolution of cluster size and other structural details provide additional insights into the later stages of the polymerization process. Thermodynamic and kinetic data are extracted and compared with previously published experimental values.

Our motivation in this study is to evaluate current prospects for the direct simulation of sol−gel processing using standard molecular simulation techniques and potentials that could, in principle, be fit to purely ab initio calculations. One could then simulate these systems without fitting either the dynamics or the potentials to experimental data or understanding. While the FG potential model is primitive by modern standards (it contains neither charge-transfer terms nor polarizabilities), it remains the only reactive potential available that describes both dissociable water and silica polymorphs, although we note that the recently introduced ReaxFF force fields[56] could be extended to these systems in a straightforward way. We anticipate that the results of these simulations will be useful both for the rather direct picture they afford of the oligomerization process and also as a reference against which to test diffusive DMC simulations and other methods developed to access longer time-scales.

II. Computational Procedures

II.1. Potentials. The Feuston and Garofalini (FG) interatomic potential for Si, O, and H[26] is an entirely atomic model (e.g., it

makes no distinction between the interactions between "bonded" and "nonbonded" atoms) that includes both two-body and three-body interactions as follows

$$V(\{\mathbf{r}\}) = \sum_{i,j} V_2(\mathbf{r}_i,\mathbf{r}_j) + \sum_{i,j,k} V_3(\mathbf{r}_i,\mathbf{r}_j,\mathbf{r}_k), \quad \{\mathbf{r}\} = (\mathbf{r}_1,\mathbf{r}_2,\mathbf{r}_3,...,\mathbf{r}_N) \tag{3a}$$

$$V_2(\mathbf{r}_i,\mathbf{r}_j) = V^{\mathrm{BMH}}(r_{ij}) + \sum_k V_k^{\mathrm{RSL2}}(r_{ij}) \tag{3b}$$

$$V^{\mathrm{BMH}}(r_{ij}) = A_{ij}\exp\left(\frac{-r_{ij}}{\rho_{ij}}\right) + \frac{Z_i Z_j}{r_{ij}}\,\mathrm{erfc}\left(\frac{r_{ij}}{\beta_{ij}}\right) \tag{3c}$$

$$V^{\mathrm{RSL2}}(r_{ij}) = \frac{a_{ij}}{1+\exp(b_{ij}(r_{ij}-c_{ij}))} \tag{3d}$$

$$V_3(\mathbf{r}_i,\mathbf{r}_j,\mathbf{r}_k) = \upsilon_3(r_{ij},r_{ik},\theta_{jik}) + \upsilon_3(r_{jk},r_{ji},\theta_{kji}) + \upsilon_3(r_{ki},r_{kj},\theta_{ikj}) \tag{3e}$$

$$\upsilon_3(r_{ij},r_{ik},\theta_{jik}) = \lambda_{jik}\exp\left[\frac{\gamma_{ij}}{r_{ij}-r_{ij}^\circ}+\frac{\gamma_{ik}}{r_{ik}-r_{ik}^\circ}\right]\times (\cos\theta_{jik}-\cos\theta_{jik}^\circ)^2, \quad r_{ij}<r_{ij}^\circ \text{ and } r_{ik}<r_{ik}^\circ$$
$$= 0, \quad r_{ij}\geq r_{ij}^\circ \text{ or } r_{ik}\geq r_{ik}^\circ \tag{3f}$$

The unmodified BMH potential contains a short-ranged repulsion term and a long-range Coulomb term. Normally, the Coulombic interactions would be treated using the Ewald sum[22,46,48] or other methods. Coulombic interactions are here described using a short-ranged potential consisting of the real-space part of the conventional Ewald sum, without the inverse lattice sum. This modification allows the empirical description of screening effects by treating the Ewald convergence parameter, $1/(\eta L)$, where η is the parameter controlling the rate of decay of the real-space term in the Ewald sum, as a species-dependent, size-independent adjustable parameter β_{ij}.[24,29] The resulting two-body interaction is short-ranged and can be safely truncated at a distance of 5.5 Å. The charges placed on each atom are their "formal" values; +4, −2, and +1, for Si, O, and H, respectively. The three-body term corrects the angle θ between three atoms toward an optimal angle, θ°. The range of this term is limited to neighbors within a short cutoff radius r° of the central atom i.[24]

During hydrolysis, oxygen atoms from water molecules are incorporated into the silica system. Thus, the potential must treat all oxygen atoms as interchangeable and permit the dissociation and formation of water molecules. This is accomplished by including terms from the Rahman−Stillinger−Lemberg (RSL2) potential (eq 3d);[27,51] the RSL family of models are the only widely used dissociable water models currently available. These terms describe the interaction of hydrogen atoms with other atoms in the system. We note that, because of the use of the BMH form and the screened Coulombic interaction, the pure-water part of this potential is not equivalent to the RSL2 model. Both water−water interactions and water−silicic acid interactions, as described by this potential, have been shown to be in good agreement with both ab initio calculations and experimental data.[26,27,49,57] The full parameter set can be found in ref 26.

II.2. Implementation Details. In our code, pair interactions are computed using a standard linked-list routine. A Verlet neighbor list with a radius of $\max(r_{ik}^\circ)$ is constructed for each atom during the two-body force evaluation. This list is then used to search for all contributing triples in evaluation of the three-body terms. The cost of constructing the list is negligible, and the three-body loop using the Verlet neighbor list is more easily programmed than a three-body link-list.

To further reduce computation cost, a table lookup procedure was implemented for the fast evaluation of $V(\{\mathbf{r}\})$. The tables need only be generated once. Because the two-body terms depend only on r_{ij}, one table is required for each type of (ij) interaction. The three-body term can be rewritten as a product of three scalar functions as follows:

$$\upsilon_3(r_{ij},r_{ik},\theta_{jik}) = \lambda_{jik}\exp\left(\frac{\gamma_{ij}}{r_{ij}-r_{ij}^\circ}+\frac{\gamma_{ik}}{r_{ik}-r_{ik}^\circ}\right)(\cos\theta_{jik}-\cos\theta_{jik}^\circ)^2$$
$$= \lambda_{jik}(\cos\theta_{jik}-\cos\theta_{jik}^\circ)^2 \times \exp\left(\frac{\gamma_{ij}}{r_{ij}-r_{ij}^\circ}\right)\times\exp\left(\frac{\gamma_{ik}}{r_{ik}-r_{ik}^\circ}\right)$$
$$= f(\cos\theta_{jik})\times h(r_{ij})\times h(r_{ik}) \tag{4}$$

$V_3(\mathbf{r}_i,\ \mathbf{r}_j,\ \mathbf{r}_k)$ can thus be evaluated as the product of terms obtained from three one-dimensional lookup tables. The Newton−Gregory forward difference interpolation method was used in each table lookup.[58] The grid size was taken to be 0.002 for the term containing $\cos(\theta_{jik})$, and 0.0002 Å for all other terms. Under these conditions, the typical difference in total energies obtained from table-interpolation and analytical evaluations was less than one part in 10^{10}. Forces were computed by evaluating the first derivative of the Newton−Gregory interpolator, ensuring correct energy conservation and dynamics.

II.3. Parallelization. The simulation code was parallelized using a domain decomposition algorithm in which the simulation box is divided into smaller volumes and a processor is assigned to each volume.[59,60] The Message Passing Interface (MPI) library is used to handle communications between processors. Data pertaining to atoms within a particular volume are stored only by its associated processor. This processor is also responsible for the integration of the equations of motion for these atoms, for the computation of the forces these atoms exert on each other, and for the computation of one-half of the interactions between its own atoms and those in neighboring volumes. The equations of motion are solved using a fifth-order Gear predictor-corrector integrator.[58] In the predictor step, the positions of atoms within each volume are updated by the assigned processor at the beginning of each time step. The positions of atoms within the potential range of neighboring volumes are then packed into arrays and sent to the neighboring processors. Atoms near to the corners or edges of a volume must be sent to more than one neighboring processor. Upon receipt of all messages, each processor calculates the forces associated with its "own" atoms and those just received. The partially computed force vectors are then returned to the originating processor, where they are summed to obtain the complete force on every atom in the system. Finally, the time step is completed in the corrector function. Because the potential is short-ranged, communications occur only between processors with immediately adjacent volumes. Example timings for serial and parallel variants of this program are shown in Table 1.

All simulations were carried out on a cluster of 24 dual-Athlon MP2200 servers. The servers are neworked with Gigabit Ethernet and use the LAM MPI implementation as provided

TABLE 1: Example Timings for the Variants of MD Program Used in This Study

	implementation	time per step per 10 000 atoms (s)
serial code	analytical evaluation of $V(\{\mathbf{r}\})$	0.966
serial code	table lookup	0.649
parallel code with table lookup	4 processors	0.197
	10 processors	0.076

by the OSCAR v1.4 parallel software suite. Most calculations were performed on 10 processors of this cluster.

II.4. Simulation Details. Experimentally, the polymerization of sol−gel precursors occurs on time-scales of seconds to hours, whereas the time accessible in a single MD simulation is on the order of nanoseconds. Previous studies by Garofalini et al. have demonstrated that the polymerization of silicic acid occurs on a subnanosecond time-scale at 2500 K.[27,31] Other studies have also adopted high-temperature conditions to increase the rates of reaction.[16,17,31,49] The simulations presented here were performed at 2500 K unless otherwise specified. The initial configuration for each simulation was constructed by distributing 729 $Si(OH)_4$ molecules in a ($9 \times 9 \times 9$) simple cubic array, except for simulations at 17 wt % silicic acid (the most dilute solution), where a ($6 \times 6 \times 6$) simple cubic array was used. Water molecules were then added to the system to achieve the desired solution density and water-to-silicon ratio, *r*. The final density of each system (unless otherwise specified, see Results) was 1.0 g/cm^3. These initial configurations were allowed to relax at 300 K for 10 ps before raising the temperature to a high value. This relaxation allows the silicic acid molecules to diffuse to a reasonably random configuration. Results obtained in the simulation studies described above suggest that this equilibration period should be sufficient; this was confirmed by visual inspection. The temperature of the system was controlled using a Gaussian-constraint isokinetic thermostat,[58] which is similar to a velocity-rescaling procedure but makes only the smallest perturbation to the trajectory necessary to keep the kinetic energy constant. A time step of 1.0 fs was used.

III. Results

We have simulated systems at varying total silicic acid concentration, water concentration, and temperature. To study the effect of excess water on the polymerization process, four concentrations were chosen, labeled I, II, III, and IV. At each concentration, two initial configurations were constructed as above. The first, "a" system, consisted of silicic acid and water at the desired concentration. The second, "d" system, consisted only of silicic acid at the same number density as in the "a" system. The effect of temperature on the polymerization process was also studied. MD simulations of "a" systems at each concentration were carried out at different temperatures, labeled "b" and "c". A complete list of the systems studied is shown in Table 2. The simulations discussed below comprise a total computational cost of approximately 10^{12} atom-time-steps. This is substantially greater than those in prior simulation studies of these potentials,[26,31,49] which have tended to run to around 3×10^9 atom-time-steps. The large cost of these simulations is due principally to a combination of longer runs and the inclusion of solvent, which raises the total number of particles simulated to as many as 30 000.

III.1. Polymerization of Silicic Acid in Water. A simulation of 34.8 wt % $Si(OH)_4$ in H_2O (system II.a) was carried out as described in section II. This weight percent corresponds to a water-to-silicon ratio, *r*, of 11. The total simulation time was 12 500 ps (12.5 million steps) at 2500 K, which makes this the longest trajectory simulated in this work. A series of snapshots from the first 5 ns of this simulation are shown in Figure 1. As is clearly evident from these visualizations, even within the first nanosecond of simulation time, a substantial number of silica dimers have formed, as well as smaller numbers of a distribution of larger species. In the second and third snapshots, at 2 and 3 ns, respectively, both "compact" and "noncompact" clusters are present, while by the final snapshot the overall impression is of a distribution of relatively compact clusters, with one large structure clearly visible that might be the result of the aggregation of several smaller clusters.

The time evolution of the percentage population of each of the Q_n species in this simulation is shown in Figure 2. These data are measured from individual simulation snapshots; oxygen atoms are identified as "bridging" if they are part of a Si−O−Si group with both Si−O distances within the cutoff range of the three-body potential. The relative population of Q_0 decreases with time, as silicic acid monomers are incorporated into clusters. A cluster is defined as a structure containing two or more silicon atoms, and the cluster size is the number of silicon atoms it contains; all Q_x with $x > 0$ are clearly part of a cluster. The relative population of Q_1 reaches a broad maximum between short times and approximately 2500 ps. Q_1 species are silicon

TABLE 2: List of Solutions Studied

solution	concentration (wt %)	$Si(OH)_4$ density (g/cm^3)	H_2O:Si ratio	temperature (K)	simulation time (ps)
I.a	17.0	0.170	26	2500	8200
I.b	17.0	0.170	26	2000	1600
I.c	17.0	0.170	26	1500	1600
I.d	100.0	0.170	0	2500	5000
II.a	34.8	0.348	11	2500	12 500
II.b	34.8	0.348	11	2000	1600
II.c	34.8	0.348	11	1500	1600
II.d	100.0	0.348	0	2500	5000
II.e	59.5	0.348	4	2500	1600
II.f	42.3	0.348	8	2500	1600
III.a	64.0	0.640	3	2500	8000
III.b	64.0	0.640	3	2000	1600
III.c	64.0	0.640	3	1500	1600
III.d	100.0	0.640	0	2500	5000
IV.a	100.0	1.000	0	2500	8000
IV.b	100.0	1.000	0	2000	1600
IV.c	100.0	1.000	0	1500	1600

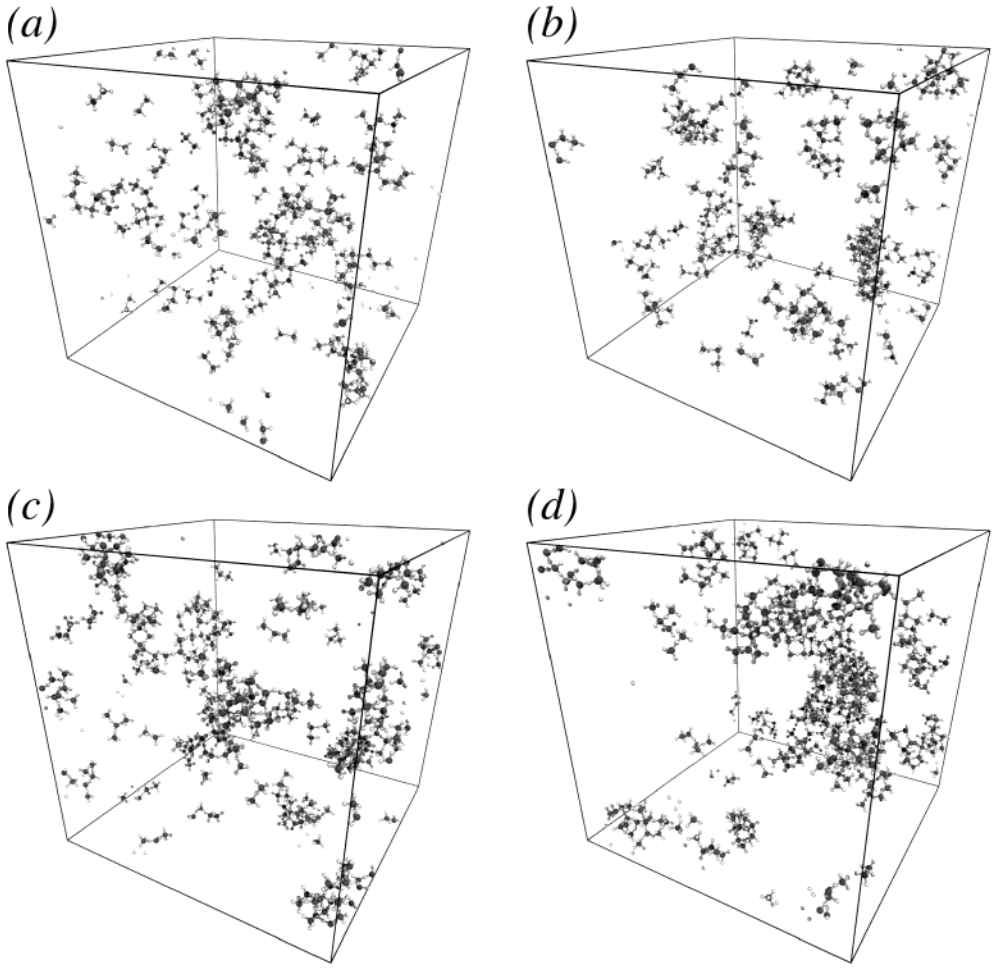

Figure 1. Simulation snapshots of polymerization in solution II.a. Only silica polymorphs containing at least two silicon atoms are shown; all silicic acid monomers and water molecules (which completely fill the remainder of the simulation cell) are removed for clarity. Only silicon and oxygen atoms are shown; terminal hydrogens have been removed. Snapshots are taken from the simulation at times (a) 1.0 ns, (b) 2.0 ns, (c) 3.0 ns, and (d) 4.8 ns.

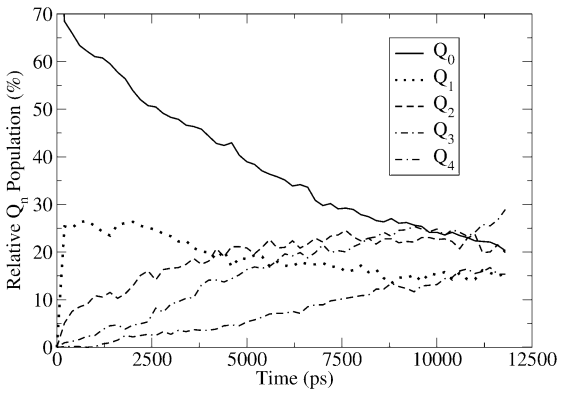

Figure 2. Relative Q_n population as a function of time in solution II.a. The relative Q_n population is determined as $N(Q_n)/N(\text{total Si}) \times 100\%$.

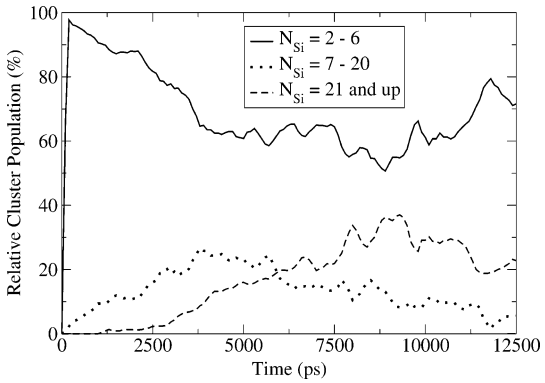

Figure 3. Cluster size distribution of solution II.a, as a function of time. The percentage is calculated as the number of clusters of size *x* divided by the total number of clusters in the solution at a given instant, times 100%.

atoms with only one bridging oxygen attached and represent the terminal silicon atoms in a cluster. The short-time rise in Q_1 is consistent with a rapid reaction of monomers to form dimers, in which both silicons are terminal. Figure 3 shows the cluster size distribution as a function of time. These data were obtained by analysis of individual snapshots via a recursive cluster-counting algorithm. By comparing Figures 2 and 3, one can see that the population of small clusters (dominated by the dimers) reaches a maximum very quickly, after which the population of "small" clusters drops steadily and the number of larger clusters formed in the solution increases rapidly, as seen in the snapshots of Figure 1. This type of behavior is also seen in experimental NMR studies.[1−3,5,6] The rise in the percentage population of small clusters at very late times is due only to the steady decline of the total number of clusters, rather than to any additional production mechanism.

Q_2 species are characteristic of linear ("chain-like") structures. As in previous studies,[31] the population of Q_2 species passes through a maximum during the polymerization process. The maximum Q_2 population occurs at approximately 8250 ps in

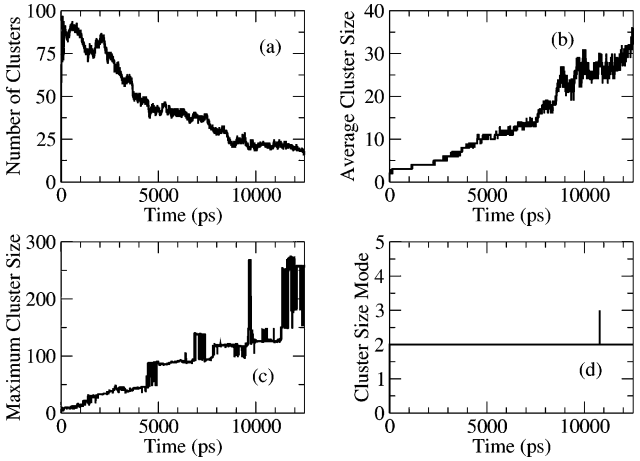

Figure 4. (a) Time evolution of the number of total clusters present in solution II.a. (b) Time evolution of the average cluster size in solution II.a. The average cluster size is given by the total number of silicon atoms that have been polymerized divided by the total number of clusters in the solution at a given instant. (c) Time evolution of maximum cluster size in solution II.a. (d) Time evolution of the mode (the most frequently encountered value) of the cluster size in solution II.a.

this simulation (Figure 2). Computer graphics visualizations (Figure 1) confirm that as clusters become larger, they contain a higher degree of cross-linking, resulting in a more compact structure with fewer terminal silicons. The Q_2 maximum coincides roughly with the maximum fraction of "large" (over 21 silicon atoms) clusters, visible in Figure 3. However, the maximum in the fraction of large clusters is due to the aggregation of large clusters in the late stages of polymerization, as discussed below.

The time evolution of several measures of the cluster size in system II.a are shown in Figure 4. The number of clusters (Figure 4a) grows very rapidly during the first several picoseconds of the simulation, and then decays slowly. The average cluster size grows (Figure 4b and c) throughout the simulation. The most frequently occurring cluster size (the mode, Figure 4d) remains at two throughout the simulation, indicating a large relative population of silicic acid dimer even at very late times. This observation is consistent with the Q_1 data shown above and is also in qualitative agreement with published NMR data which have suggested that silicic acid dimer exists in high concentration in aqueous silicic acid solutions, while cyclic trimers are more commonly found in basic solutions.[1,5,11]

Due to the small size of the simulation cell, the maximum cluster size fluctuates strongly throughout the simulation (Figure 4c); this occurs because the maximum cluster size, by definition, is not an "average" property but instead depends strongly on the behavior of a single cluster. The magnitude of this fluctuation is small early in the simulation (when the cluster size distribution is very narrow) and increases as the number of clusters in the solution decrease. The smaller magnitude changes are the result of monomers or small clusters being incorporated into (or dissociated from) a large cluster, whereas large changes occur when two large clusters condense or when a large cluster fragments into smaller ones. The large fluctuations in the maximum cluster size observed later in the simulation suggest that the growth mode of clusters shifts from a (monomer or dimer)−cluster aggregation mechanism to a cluster−cluster aggregation mechanism. At times of approximately 4500, 7000, 9500, and 11 000 ps, the maximum cluster size appears to oscillate between two very different values for a period of tens to hundreds of picoseconds before stabilizing. This suggests that the colliding clusters separate and rejoin several times before forming a strong bond and that cluster−cluster aggregation in this system is a reversible process even on the time-scale accessible to molecular dynamics simulations. Again, changes in the maximum cluster size are changes in the size of a single cluster and therefore reflect the making and breaking of individual bonds. The average cluster size data (Figure 4d) are also indicative of cluster−cluster aggregation; at late times, the average cluster size increases at a higher rate than at short times. Because the supply of monomer is quite depleted at late times, this behavior is best explained by the aggregation of clusters to form much larger clusters.

The smaller clusters visualized in Figure 1 tend to be quite compact, while the larger ones have more complex structures. We have directly measured the largest cluster observed, a snapshot of which is shown in Figure 5. Visually, the cluster appears to be dense, but of a shape likely produced by the aggregation of several smaller spheroid clusters. The length of the cluster is 67.2 Å, which is 97% of the simulation box length. The radius of gyration of this structure, which measures the distance between each atom and the center of mass, is calculated to be 24.1 Å, suggesting that most of the atoms are far from the cluster center. It is unfortunately not possible to obtain meaningful mass- or surface-fractal dimensions from such a small object, although this might be possible in future studies of substantially larger systems. The compactness of the smaller clusters observed in Figure 1 is consistent with a growth model which allows for substantial intracluster relaxation and bond formation, which is consistent with the high temperature and low activation energy of bond formation (see below) in this system. The aggregate structures observed at late times are reminiscent of the products of various cluster−cluster aggregation models. However, the reversibility of bond formation between large clusters (described above) and the relaxation of cluster structure upon bonding (presumably active based on the compact structures of the smaller clusters) are not included in either reaction-limited or diffusion-limited cluster−cluster aggregation (RLCA and DLCA, respectively) models[61] for gel formation, so no detailed comparison can be made.

Prior studies have suggested that polymerization occurs initially through the formation of linear clusters rather than cyclic clusters.[12,27,49] [The focus here is on clusters with three or more silicons, because clusters containing only two silicons are trivially linear.] They have also suggested that although cyclic structures containing three silicon atoms are possible, they are not energetically favorable with respect to rings containing four or five silicon atoms.[1,11,12,41] The ring size analysis of clusters in system II.a is shown in Figure 6 and indicates that at short times (500 ps) four-membered rings are more common than any other cyclic structure. Note that the ring-counting algorithm we have used detects all rings, rather than "irreducible" ones, which leads to large numbers of rings with large *N*. At all times after 500 ps, though, a clear peak is observed at five silicons, and there are relatively few three- and four-silicon rings. This result is also consistent with previous investigations.[27,49]

III.2. Effects of Concentration on the Polymerization of Silicic Acid Solutions. The time evolution of the fraction of silicic acid that has reacted and the number of siloxane bridges formed, at several concentrations, are plotted in Figure 7. When only a small amount of water is present initially, that is, $r \leq 3$, systems III.a and IV.a, about 60% of silicic acid monomers react in the first 100 ps, after which the rate of polymerization (the time derivative of these data) decreases drastically. By examining the relative cluster populations (Figure 8), one can see that

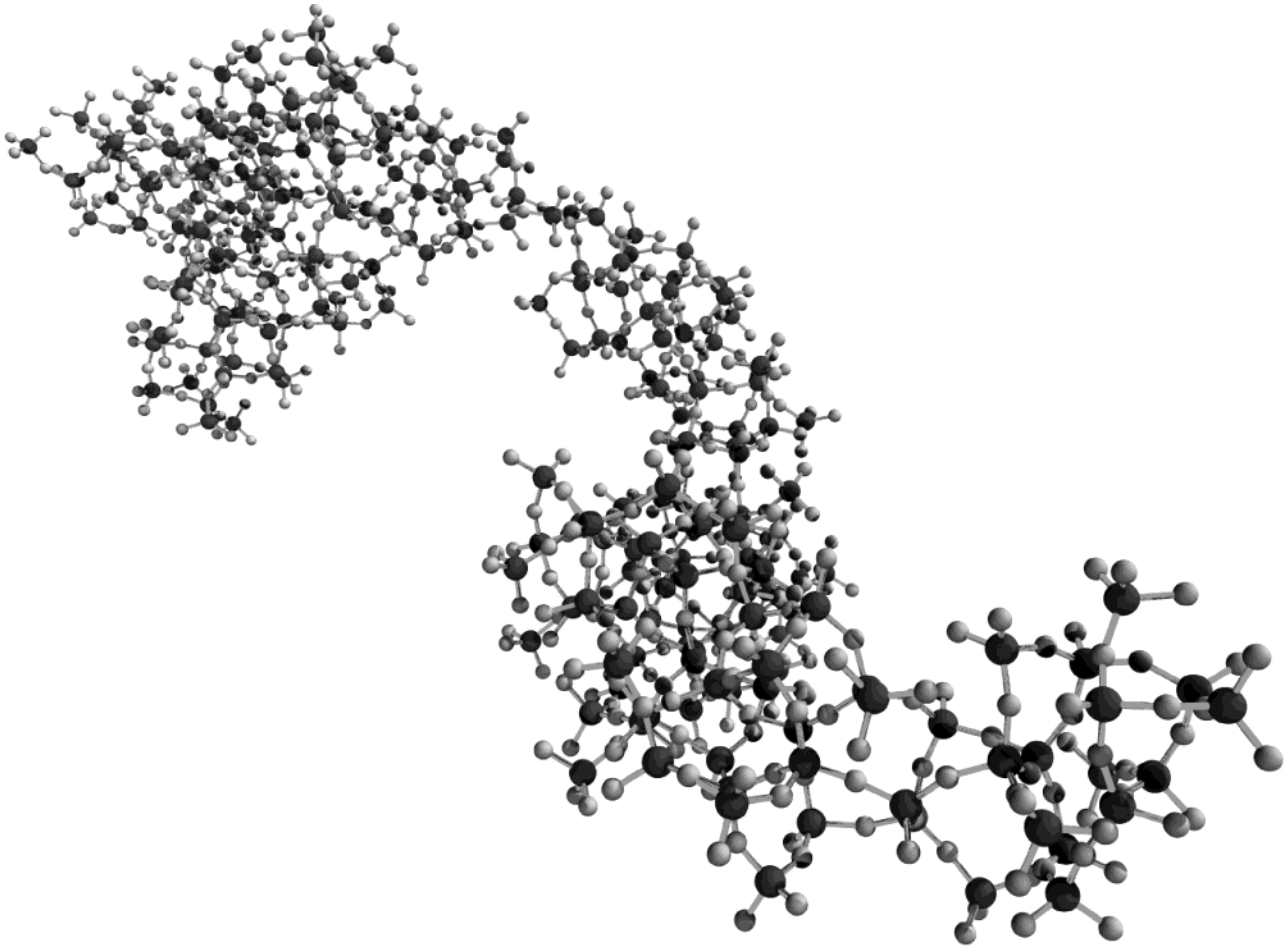

Figure 5. Snapshot of the largest cluster formed in solution II.a after 12.5 ns of simulation.

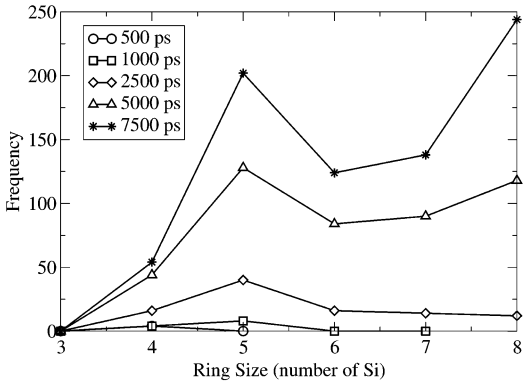

Figure 6. Distribution of ring sizes in simulation II.a at different times. The size of a ring is the number of silicon atoms it contains. Note that large rings may be "reducible" into smaller ones; this is not taken into account in our analysis.

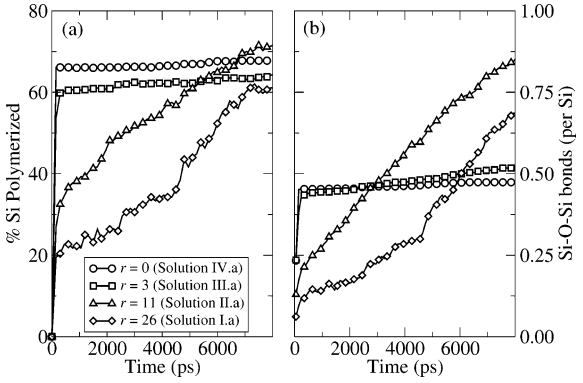

Figure 7. (a) Percentage of silicic acid monomers polymerized in solutions I.a, II.a, III.a, and IV.a. This percentage is calculated by dividing the total number of silicon atoms in clusters at a given instant by the total number of silicon atoms in solution, times 100%. This quantity is reported as a percentage because solutions of concentration I (17% silicic acid by weight) contain only 216 silicic acid monomers, whereas all other solutions contain 729 silicic acid monomers. (b) Number of silane bonds formed, per silicon atom, in the same solutions. This is simply the number of Si−O−Si bonds identified (as explained in the text) divided by the total number of silicon atoms present. Note that each bond involves two silicon atoms.

more than 90% of the clusters formed in these systems contain no more than six silicon atoms. At late times the population of large (21 silicons or more) clusters is effectively flat, and the number of medium-sized clusters increases slowly while the number of small clusters decreases. Because the fraction of silicic acid polymerized remained nearly constant, the changes in size distribution data suggest that the small clusters are aggregating to form medium-sized clusters. At lower concentrations ($r = 11$ and 26), polymerization occurs more slowly during the first 100 ps, but more quickly at later times. Figure 8 shows that the medium- and large-sized clusters in these systems constitute a significant fraction of all clusters present in the solution. The continued growth in the fraction of silicic acid reacted at low concentrations (Figure 7) suggests that in these systems both monomer incorporation and cluster−cluster aggregation mechanisms are active. The rate of polymerization at $r = 11$ and 26 begins to decrease after 7 ns, but equilibrium is clearly not reached in either of these simulations.

The presence of water appears to promote the formation of cyclic clusters (Figure 9). When no water is present in the initial

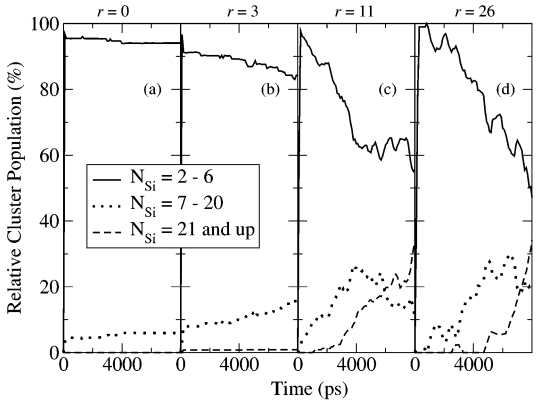

Figure 8. Cluster size distributions as a function of time for solutions (a) IV.a, (b) III.a, (c) II.a, and (d) I.a. The plots are arranged in increasing order of *r*. The cluster size distributions are calculated as described in Figure 3.

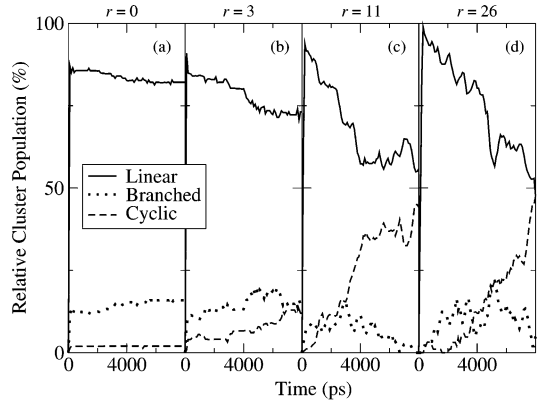

Figure 9. Cluster-type distributions as a function of time for solutions (a) IV.a, (b) III.a, (c) II.a, and (d) I.a. The plots are arranged in order of increasing *r*. The percentage of each cluster type is calculated by dividing the number of clusters of that type by the total number of clusters present in the solution at a given instant, times 100%.

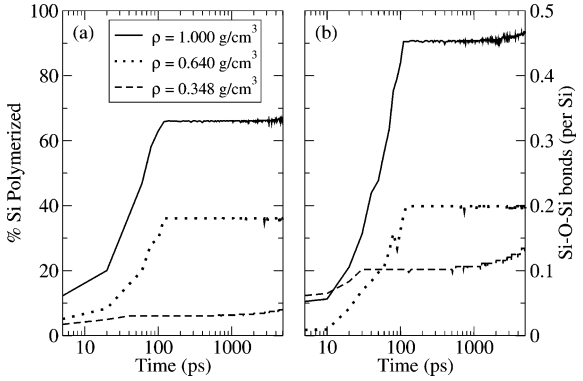

Figure 10. (a) Percentage of silicic acid monomers polymerized in solutions II.d, III.d., and IV.a, as defined in the caption to Figure 7. (b) Number of silane bonds formed, per silicon atom, in the same solutions. In simulating system I.d (not shown), no significant polymerization was observed. The plots are arranged in increasing order of *r*.

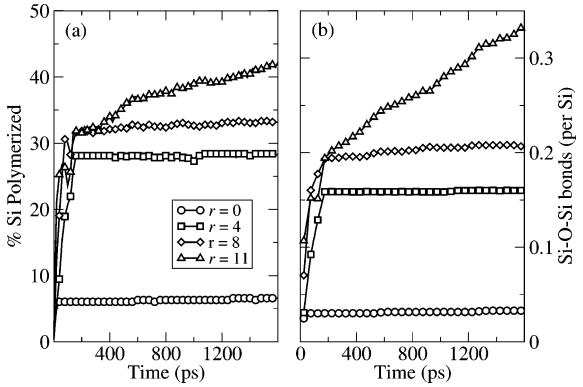

Figure 11. (a) Percentage of silicic acid monomers polymerized in solutions II.a, II.d, II.e, and II.f. (b) Number of silane bonds formed, per silicon atom, in the same solutions. Percentages are calculated as described in Figure 7.

configuration ($r = 0$), only 2% of the clusters formed during the polymerization process contain cyclic structures. When $r = 3$, the percentage of cyclic clusters present at the end of the simulation increases to 4%. Both of these measures are consistent with the very low fraction of large clusters; when most clusters contain only two or three silicons, hardly any will be cyclic or branched. When the value of *r* is increased to 11, nearly one-half of the clusters formed contain cycles by the end of simulation. Inspection of Figures 8 and 9 indicates that the fraction of cyclic structures tracks the fraction of "large" clusters quite well, suggesting that cyclization occurs principally within large clusters. This is consistent with the compact cluster structures discussed earlier and probably results from intracluster bond formation. As discussed below, water catalyzes both the condensation reaction 1 and the reverse reaction (hydrolysis), so that the presence of water may facilitate intramolecular rearrangements in large clusters by successive hydrolysis and condensation reactions. Previous studies have also suggested that hydrolysis reactions redistribute the silanol bonds to maximize the number of bridging oxygens in each cluster, which favors the formation of compact clusters with more ring structures.[13]

The effect of water is further studied by removing all of the water in several of the initial configurations while keeping the number of silicic acid monomers and the simulation box size constant (Figure 10). The densities of the resulting systems are 0.384, 0.64, and 1.00 g/cm^3. The rate and extent of polymerization is strongly dependent on the density, with high-density systems polymerizing much more quickly than low-density systems, almost certainly because of the much higher collision frequency in the denser systems. The low degree of polymerization in these systems as compared with the others suggests that water acts as a catalyst which facilitates the condensation reaction.[1,11] The catalytic nature of water is further studied by varying the number of water molecules initially present while keeping the silicic acid density constant at 0.384 g/cm^3. Figure 11 shows that, at constant silicic acid density, by increasing *r* from 0 to 4 the percentage of reacted monomers is increased from 6% to 28% at 400 ps. At later times, as well, the presence of large quantities of water clearly facilitates further reaction; for $r = 11$, monomers continue to react at a high rate until at least 1600 ps, while in the other three systems reactions continue but only much more slowly. These results are consistent with the picture derived from experimental results on TEOS polymerization at varying water concentration and acidic conditions.[63,34]

Water is also a product of the condensation reaction 1, and in an equilibrium system one might expect the presence of additional water to shift the equilibrium back toward reactants via hydrolysis. Because the condensation (1) is isodesmic and has no net change in the number of moles, solvation energies are likely a major contributor to the overall reaction free energy. The presence of excess water may substantially shift the equilibrium to the right if the solvation free energy (under these conditions) of the reactants is more positive than that of the

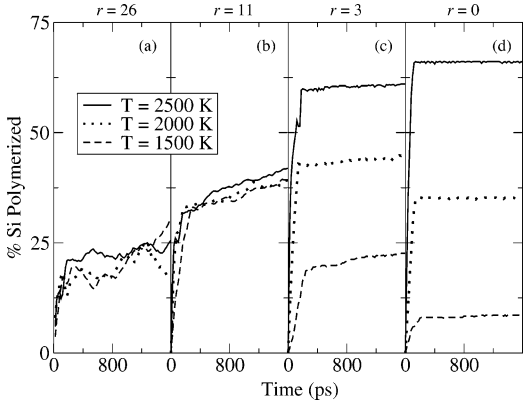

Figure 12. Percent of silicic acid monomers polymerized in solutions (a) I.a, b, and c, (b) II.a, b, and c, (c) III.a, b, and c, and (d) VI.a, b, and c. Percentages are calculated as described in Figure 7.

products. Of course, under the conditions simulated here, the solvent, although of similar density to ambient water, is highly supercritical, which should be expected to substantially impact such solvation free energies.

III.3. Effects of Temperature on Polymerization. The relative populations of polymerized silicic acid in solutions of different concentrations at 1500, 2000, and 2500 K are plotted in Figure 12. As expected, the reaction rate increases as temperature increases. Several additional 1500 ps simulations were carried out at 300 and 600 K. No polymerization was observed in these. For $r = 11$ (Figure 12b), the rate of polymerization is a function of temperature for the first 300 ps of simulation, but at later times the fraction of polymerized monomer increases at essentially the same rate at all three temperatures. This suggests that later-stage cluster growth is diffusion-limited; the diffusion rate is determined principally by the density, which is constant. Similar trends are observed when $r = 26$ (Figure 12a). In the cases of $r = 3$ and $r = 0$ (Figure 12c,d), the polymerization depends more strongly on the temperature. The fraction of monomers reacted increases rapidly during the first 200 ps, and many more react at 2500 K than at the lower temperatures. The temperature dependence of the extent of reaction at $r = 0$ could be taken to suggest that under these reaction conditions the reaction is endothermic by approximately 20 kcal/mol. However, the condensation of isolated monomers has been shown to be exothermic, with a net energy change estimated at -9.3 kcal/mol by quantum-mechanical studies;[44] the original studies of the FG potential[26] estimated this value to be -7.4 kcal/mol in this model. One possible resolution for this discrepancy is that the very low water concentration makes the reverse reaction unlikely on the time-scales observed here (the forward reaction has a lower activation energy and is still observed), so that even though the extent of reaction has stabilized it is not at equilibrium and the temperature dependence of the extent of reaction is not meaningful. Another possibility is that intermolecular interactions in these systems lead to a positive change in solvation enthalpy during reaction, which outweighs the intramolecular contribution.

Quantum-mechanical studies have estimated the activation energy of condensation between two monomers to be between 12 and 15 kcal/mol.[19,21,39] Previous studies using the FG potential have reported that at a density of 1.6 g/cm^3, the activation energy of condensation between two silicic acid monomers is 23 kcal/mol at 2500 K.[31] The experimentally determined value for this quantity is around 15 kcal/mol (14.6 kcal/mol at pH = 4; this value is extracted from a kinetic analysis of a series of condensation reactions rather than initial-rate data[11,64]). We have estimated the activation energies of this reaction in our simulations to be 13 kcal/mol at $r = 26$, 15 kcal/mol at $r = 11$, 24 kcal/mol at $r = 3$, and 20 kcal/mol at $r = 0$. The rate constant k was estimated by fitting the population of monomer during the first 35 ps of each simulation to a second-order decay. The activation energy E_a was then estimated from the slope of a plot of ln k versus $1/T$. The solvent clearly plays an important role in the reaction dynamics. The large discrepancy between the experimentally determined value and the previous simulation results is explained by the lack of solvent in the earlier simulations. The activation energies obtained in this work at $r = 26$ and $r = 11$ are in good agreement with the experimental values; these water-to-silicon ratios are comparable with those used in many experimental studies. Extrapolation of our kinetic data to predict the rate constant for the condensation of two monomers at 300 K yields a value of 0.23 min^{-1}. At a pH of 3.8, the rate constant for this reaction is experimentally determined to be 0.03 min^{-1}.[11,65] Given unavoidable differences between the pH and other properties of the simulated systems and experiments and extrapolation of the Arrhenius law over more than 1200 K, the agreement between our simulated and experimental rate constants is quite good. Using the same data, we estimate that the time required for 0.5% of the monomer to condense is around 0.02 s in the model system; this time-scale of which is not accessible to present MD techniques.

IV. Conclusion

The polymerization of silicic acid in aqueous solution has been studied using molecular dynamics simulations. The structural details of clusters formed in the presence of excess water are in qualitative agreement with experimental NMR data. When the water-to-silicon ratio is sufficiently large, the polymerization is reaction-limited only in the initial stages, which are dominated by the formation of dimers. Cluster−cluster aggregation events are clearly visible even on a molecular simulation time-scale. The water model used here appears to be quite acidic, in terms of both its dissociability and the effect it has on silicic acid polymerization. Water clearly acts as a catalyst in the condensation reaction. The activation energy of condensation between monomers is estimated to be 13−15 kcal/mol in the presence of excess water, which is in good agreement with an experimental value of 15 kcal/mol; extrapolation of simulated kinetic data to 300 K is in agreement with experimental data to within one order of magnitude. Simulations of the type performed here can be useful in understanding gelation kinetics and thermodynamics, for developing a complete understanding of the microscopic structures formed during gelation, and, if performed on a substantially larger scale, for the preparation of atomistic models of xerogels and aerogels which could be used in further "application" simulations, for instance, of chromatography. Furthermore, the model used here can be further refined and easily extended to other inorganic oxide gel systems. Last, the atomic-scale structural information available from simulations such as these could be used to both validate and parametrize simulations using long-time methods such as Dynamic Monte Carlo, which are the most suitable way to directly simulate gelation under ambient conditions.

Acknowledgment. We wish to acknowledge the National Science Foundation for support of this work through grant no. CHE-0241005.

References and Notes

(1) Brinker, C. J.; Scherer, G. W. *Sol−Gel Science: The Physics and Chemistry of Sol−Gel Processing*; Academic Press: London, 1989.

(2) Brunet, F.; Cabane, B. Populations of Oligomers in Sol−Gel Condensation. *J. Non-Cryst. Solids* **1993**, *163*, 211−225.

(3) Devreux, F.; Boliot, J. P.; Chaput, F.; Lecompte, A. Sol−Gel Condensation of Rapidly Hydrolyzed Silicon Alkoxides − a Joint ^{29}Si NMR and Small-Angle X-ray-Scattering Study. *Phys. Rev. A* **1990**, *41*, 6901−6909.

(4) Wijnen, P. W. J. G.; Beelen, T. P. M.; Vansanten, R. A. Silica-Gels from Aqueous Silicate Solutions − Combined ^{29}Si NMR and Small-Angle X-ray-Scattering Spectroscopic Study. *Colloid Chem. Silica* **1994**, 517−531.

(5) Knight, C. T. G.; Thompson, A. R.; Kunwar, A. C.; Gutowsky, H. S.; Oldfield, E.; Kirkpatrick, R. J. ^{17}O Nuclear Magnetic-Resonance Spectroscopic Studies of Aqueous Alkaline Silicate Solutions. *J. Chem. Soc., Dalton Trans.* **1989**, 275−281.

(6) Kinrade, S. D.; Swaddle, T. W. ^{29}Si NMR Studies of Aqueous Silicate Solutions. 1. Chemical Shifts and Equilibria. *Inorg. Chem.* **1988**, *27*, 4253−4259.

(7) Kinrade, S. D.; Swaddle, T. W. ^{29}Si NMR Studies of Aqueous Silicate Solutions. 2. Transverse ^{29}Si Relaxation and the Kinetics and Mechanism of Silicate Polymerization. *Inorg. Chem.* **1988**, *27*, 4259−4264.

(8) Wijnen, P. W. J. G.; Beelen, T. P. M.; Rummens, C. P. J.; van Santen, R. A. Diffusion-Limited and Reaction-Limited Aggregation of Aqueous Silicate Solutions. *J. Non-Cryst. Solids* **1991**, *136*, 119−125.

(9) Beelen, T. P. M.; Wijnen, P. W. J. G.; Vonk, C. G.; van Santen, R. A. SAXS Study of Silica-Gel Formation from Aqueous Silicate Solutions. *Catal. Lett.* **1989**, *3*, 209−215.

(10) Kelts, L. W.; Armstrong, N. J. A ^{29}Si NMR Study of the Structural Intermediates in Low pH Sol−Gel Reactions. *J. Mater. Res.* **1989**, *4*, 423−433.

(11) Iler, R. K. *The Chemistry of Silica*; John Wiley and Sons: New York, 1979.

(12) Hench, L. L.; West, J. K. The Sol−Gel Process. *Chem. Rev.* **1990**, *90*, 33−72.

(13) Klemperer, W. G.; Mainz, V. V.; Millar, D. M. A Molecular Building-Block Approach to the Synthesis of Ceramic Materials. In *Better Ceramics Through Chemistry II*; Brinker, C. J., Clark, D. E., Ulrich, D. R., Eds.; Materials Research Society: Pittsburgh, PA, 1986; pp 3−13.

(14) Brinker, C. J.; Keefer, K. D.; Schaefer, D. W.; Assink, R. A.; Kay, B. D.; Ashley, C. S. Sol−Gel Transition in Simple Silicates II. *J. Non-Cryst. Solids* **1984**, *63*, 45−59.

(15) Athanasopoulos, D. C.; Garofalini, S. H. Molecular-Dynamics Simulations of the Effect of Adsorption on SiO_2 Surfaces. *J. Chem. Phys.* **1992**, *97*, 3775−3780.

(16) Brodka, A.; Zerda, T. W. Molecular-Dynamics of SF_6 in Porous Silica. *J. Chem. Phys.* **1991**, *95*, 3710−3718.

(17) Brodka, A.; Zerda, T. W. Molecular-Dynamics Simulation of Reorientational Motion of SF_6 in Porous Sol−Gel Glass. *J. Non-Cryst. Solids* **1992**, *139*, 215−221.

(18) Burggraf, L. W.; Davis, L. P. A Theoretical Study of Silanol Polymerization. In *Better Ceramics Through Chemistry II*; Brinker, C. J., Clark, D. E., Ulrich, D. R., Eds.; Material Research Society: Pittsburgh, PA, 1986; pp 529−542.

(19) Burggraf, L. W.; Davis, L. P.; Gordon, M. S. Neutral and Anionic Hypervalent Silicon Complexes in Silanol Polymerization. In *Ultrastructure Processing of Advanced Ceramics*; Uhlmann, D. R., Ulrich, D. R., Eds.; John Wiley and Sons: New York, 1992; pp 47−55.

(20) Damrauer, R.; Burggraf, L. W.; Davis, L. P.; Gordon, M. S. Gas-Phase and Computational Studies of Pentacoordinate Silicon. *J. Am. Chem. Soc.* **1988**, *110*, 6601−6606.

(21) Davis, L. P.; Burggraf, L. W. A Theoretical Study of the Silanol Polymerization Mechanism. In *Ultrastructure Processing of Advanced Ceramics*; Machenzie, J. D., Ulrich, D. R., Eds.; John Wiley and Sons: New York, 1988; pp 376−378.

(22) Delaye, J. M.; Achille, V. L.; Ghaleb, D. Modeling Oxide Glasses with Born−Mayer−Huggins Potentials: Effect of Composition on Structural Changes. *J. Non-Cryst. Solids* **1997**, *210*, 232−242.

(23) Elanany, M.; Selvam, P.; Yokosuka, T.; Takami, S.; Kubo, M.; Imamura, A.; Miyamoto, A. A Quantum Molecular Dynamics Simulation Study of the Initial Hydrolysis Step in Sol−Gel Process. *J. Phys. Chem. B* **2003**, *107*, 1518−1524.

(24) Feuston, B. P.; Garofalini, S. H. Empirical 3-Body Potential for Vitreous Silica. *J. Chem. Phys.* **1988**, *89*, 5818−5824.

(25) Feuston, B. P.; Garofalini, S. H. Topological and Bonding Defects in Vitreous Silica Surfaces. *J. Chem. Phys.* **1989**, *91*, 564−570.

(26) Feuston, B. P.; Garofalini, S. H. Onset of Polymerization in Silica Sols. *Chem. Phys. Lett.* **1990**, *170*, 264−270.

(27) Feuston, B. P.; Garofalini, S. H. Oligomerization in Silica Sols. *J. Phys. Chem.* **1990**, *94*, 5351−5356.

(28) Feuston, B. P.; Garofalini, S. H. Water-Induced Relaxation of the Vitreous Silica Surface. *J. Appl. Phys.* **1990**, *68*, 4830−4836.

(29) Garofalini, S. H.; Melman, H. Applications of Molecular Dynamics Simulations to Sol−Gel Processing. In *Better Ceramics Through Chemistry II*; Brinker, C. J., Clark, D. E., Ulrich, D. R., Eds.; Materials Research Society: Pittsburgh, PA, 1986; pp 497−505.

(30) Garofalini, S. H. Molecular-Dynamics Computer-Simulations of Silica Surface-Structure and Adsorption of Water-Molecules. *J. Non-Cryst. Solids* **1990**, *120*, 1−12.

(31) Garofalini, S. H.; Martin, G. Molecular Simulations of the Polymerization of Silicic-Acid Molecules and Network Formation. *J. Phys. Chem.* **1994**, *98*, 1311−1316.

(32) Kubicki, J. D.; Lasaga, A. C. Molecular-Dynamics Simulations of SiO_2 Melt and Glass − Ionic and Covalent Models. *Am. Mineral.* **1988**, *73*, 941−955.

(33) Lasaga, A. C.; Gibbs, G. V. *Phys. Chem. Miner.* **1987**, *14*, 107−117.

(34) Lasaga, A. C.; Gibbs, G. V. Ab initio Quantum-Mechanical Calculations of Water-Rock Interactions − Adsorption and Hydrolysis Reactions. *Am. J. Sci.* **1990**, *290*, 263−295.

(35) Levine, S. M.; Garofalini, S. H. A Structural Analysis of the Vitreous Silica Surface via a Molecular Dynamics Computer Simulation. *J. Chem. Phys.* **1987**, *86*, 2997−3002.

(36) Litton, D. A.; Garofalini, S. H. Modeling of Hydrophilic Wafer Bonding by Molecular Dynamics Simulations. *J. Appl. Phys.* **2001**, *89*, 6013−6023.

(37) Martin, G. E.; Garofalini, S. H. Sol−Gel Polymerization − Analysis of Molecular Mechanisms and the Effect of Hydrogen. *J. Non-Cryst. Solids* **1994**, *171*, 68−79.

(38) O'Keeffe, M.; Domenges, B.; Gibbs, G. V. Ab Initio Molecular Orbital Calculations on Phosphates: Comparison with Silicates. *J. Phys. Chem.* **1985**, *89*, 2304−2309.

(39) Pereira, J. C. G.; Catlow, C. R. A.; Price, G. D. Silica Condensation Reaction: an Ab Initio Study. *Chem. Commun.* **1998**, 1387−1388.

(40) Pereira, J. C. G.; Catlow, C. R. A.; Price, G. D. Ab Initio Studies of Silica-Based Clusters. Part I. Energies and Conformations of Simple Clusters. *J. Phys. Chem. A* **1999**, *103*, 3252−3267.

(41) Pereira, J. C. G.; Catlow, C. R. A.; Price, G. D. Ab Initio Studies of Silica-Based Clusters. Part II. Structures and Energies of Complex Clusters. *J. Phys. Chem. A* **1999**, *103*, 3268−3284.

(42) Pereira, J. C. G.; Catlow, C. R. A.; Price, G. D. Molecular Dynamics Simulation of Liquid H_2O, MeOH, EtOH, $Si(OMe)_4$, and $Si(OEt)_4$, as a Function of Temperature and Pressure. *J. Phys. Chem. A* **2001**, *105*, 1909−1925.

(43) Pereira, J. C. G.; Catlow, C. R. A.; Price, G. D. Molecular Dynamics Simulation of Methanolic and Ethanolic Silica-Based Sol−Gel Solutions at Ambient Temperature and Pressure. *J. Phys. Chem. A* **2002**, *106*, 130−148.

(44) Pereira, J. C. G.; et al. Atomistic Modeling of Silica Based Sol−Gel Processes. *J. Sol.-Gel Sci. Technol.* **1997**, *8*, 55−58.

(45) Sauer, J. Molecular Models in Ab Initio Studies of Solids and Surfaces − from Ionic-Crystals and Semiconductors to Catalysts. *Chem. Rev.* **1989**, *89*, 199−255.

(46) Soules, T. F. A Molecular Dynamic Calculation of the Structure of Sodium Silicate Glasses *J. Chem. Phys.* **1979**, *71*, 4570.

(47) Soules, T. F. Computer-Simulation of Glass Structures. *J. Non-Cryst. Solids* **1990**, *123*, 48−70.

(48) Woodcock, L. V.; Angell, C. A.; Cheeseman, P. Molecular Dynamics Studies of the Vitreous State: Simple Ionic Systems and Silica. *J. Chem. Phys.* **1976**, *65*, 1565.

(49) Yamahara, K.; Okazaki, K. Molecular Dynamics Simulation of the Structural Development in Sol−Gel Process for Silica Systems. *Fluid Phase Equilib.* **1998**, *144*, 449−459.

(50) Burggraf, L. W.; Davis, L. P. In *Silanes, Surfaces, and Interfaces. Chemically Modified Surfaces Series*; Applications of MNDO Molecular Orbital Calculations to Silanol Polymerization; Leyden, D. E., Ed.; Gordon and Breach: New York, 1986; pp 157−187.

(51) Stillinger, F. H.; Rahman, A. Revised Central Force Potential for Water. *J. Chem. Phys.* **1978**, *68*, 666−670.

(52) Mikeš, J.; Dušek, K. Simulation of Polymer Network Formation by the Monte Carlo Method. *Macromolecules* **1982**, *15*, 93−99.

(53) Kasehagen, L. J.; Rankin, S. E.; McCormick, A. V.; Macosko, C. W. Modeling of First Shell Substitution Effects and Preferred Cyclization in Sol−Gel Polymerization. *Macromolecules* **1997**, *30*, 3921−3939.

(54) Rankin, S. E.; Kasehagen, L. J.; McCormick, A. V.; Macosko, C. W. Dynamic Monte Carlo Simulation of Gelation with Extensive Cyclization. *Macromolecules* **2000**, *33*, 7639−7648.

(55) Šefčík, J.; Rankin, S. E. Monte Carlo Simulations of Size and Structure of Gel Precursors in Silica Polycondensation. *J. Phys. Chem. B* **2003**, *107*, 52−60.

(56) van Duin, A. C. T.; Strachan, A.; Stewman, S.; Zhang, Q.; Xu, X.; Goddard, W. A., III. $ReaxFF_{SiO}$ Reactive Force Field for Silicon and Silicon Oxide Systems. *J. Phys. Chem. A* **2003**, *107*, 3803−3811.

(57) Newell, R. G.; Feuston, B. P.; Garofalini, S. H. The Structure of Sodium Trisilicate Glass Via Molecular- Dynamics Employing 3-Body Potentials. *J. Mater. Res.* **1989**, *4*, 434−439.

(58) Allen, M. P.; Tildesley, D. J. *Computer Simulation of Liquids*; Claredon Press: Oxford, 1987.

(59) Gelb, L. D.; Muller, E. A. Location of Phase Equilibria by Temperature-Quench Molecular Dynamics Simulations. *Fluid Phase Equilib.* **2002**, *203*, 1−14.

(60) Heffelfinger, G. S. Parallel Atomistic Simulations. *Comput. Phys. Commun.* **2000**, *128*, 219−237.

(61) Meakin, P. Formation of Fractal Clusters and Networks by Irreversible Diffusion-Limited Aggregation. *Phys. Rev. Lett.* **1983**, *51*, 1119.

(62) Keefer, K. D. Growth and Structure of Fractally Rough Silica Colloids. In *Better Ceramics Through Chemistry II*; Brinker, C. J., Clark, D. E., Ulrich, D. R., Ed.; Materials Research Society: Pittsburgh, PA, 1986; pp 295−304.

(63) Pouxviel, J. C.; Boilot, J. P.; Beloeil, J. C.; Lallemand, J. Y. NMR Study of the Sol/Gel Polymerization. *J. Non-Cryst. Solids* **1987**, *89*, 345−360.

(64) (a) Coudurier, M.; Baudru, B.; Donnet, J.-C. The Polycondensation of Disilicic Acid. I. Application of the Reaction of Formation of the Silicomoldybdenum Complex and of the Light Diffusion to the Study of Polycondensation of Disilicic Acid. *Bull. Soc. Chim. Fr.* **1971**, 3147; (b) The Polycondensation of Disilicic Acid. II. Influence of pH on the Kinetics and the Mechanism of the Reaction. Texture of the Products Formed. *Bull. Soc. Chim. Fr.* **1971**, 3154; (c) Polycondensation of Disilicic Acid. III. Influence of Concentration and Temperature on the Kinetics and Mechanism of Polycondensation of Disilicic Acid. Relation with the Texture of the Formed Products. *Bull. Soc. Chim. Fr.* **1971**, 3161.

(65) Alexander, G. B. The Polymerization of Monosilicic Acid. *J. Am. Chem. Soc.* **1954**, *76*, 2094−2096.